Estimation of K Distribution Parameters Using Neural Networks

Mark P. Wachowiak*, Renata Smolíková, Jacek M. Zurada, and Adel S. Elmaghraby

***Abstract*—The K distribution is an accurate model for ultrasonic backscatter. A neural approach is developed to estimate K distribution parameters. Accuracy and consistency of the estimates from simulated K and envelope data compare favorably with other techniques. Neural networks can potentially be used as a complementary technique for tissue characterization.**

***Index Terms*—K distribution, neural networks, parameter estimation, speckle, ultrasonography.**

I. Introduction

Models of ultrasonic backscatter, specifically of the echo envelope of the demodulated radio-frequency (RF) signal, can provide clinically useful information about the regularity and density of scatterers (small structures in tissues, such as cells), and can be useful in diagnosis and pathology analysis [1]–[3]. In ultrasonography, first-order envelope statistics have been thought to follow a Rayleigh distribution, but recent work has shown that more general models, such as the Nakagami, K, generalized K, and homodyned K distributions better describe envelope statistics [2]–[6].

The present preliminary study presents the use of artificial neural networks (ANNs) to estimate the shape parameter of a specific backscattering model, the K distribution. Estimates computed directly from moments may be inaccurate and heavily influenced by outliers, especially for small sample sizes. Additionally, many current techniques require numerical solutions to complex equations. To address these issues, an alternative approach based on ANNs was developed. Desirable features of ANNs are: 1) nonlinearity, for good data fit; 2) robustness in the presence of noisy and inaccurate measurements; 3) generalization and adaptation; and 4) parallelism that can be implemented in hardware [7]. Estimation is formulated as a function approximation problem, to which ANNs are particularly well suited [7], [8].

II. A Scattering Model Based on the K Distribution

The K distribution is a model for a small number of randomly spaced scatterers and clustered scattering. It also encompasses pre-Rayleigh [signal-to-noise ratio (SNR) less than 1.91] and Rayleigh (SNR $\approx$ 1.91) conditions. It is particularly accurate for densities in the range of 9 to 12 [2]. The model is completely specified by shape parameter ν and scale parameter a, with probability density function (PDF) [9]

$$f_X(x) = \frac{2}{a\Gamma(\nu+1)}\left(\frac{x}{2a}\right)^{\nu+1} K_\nu\left(\frac{x}{a}\right), \quad x \geq 0, \quad \nu > -1, \quad a > 0 \tag{1}$$

where x denotes the amplitude of the envelope, $\Gamma(\cdot)$ denotes the gamma function, and $K_\nu(\cdot)$ is the modified Bessel function of the second kind and order ν. From the data and the ν estimate, a can then be calculated [1], [9]. Plots of the K PDF for various ν and for unit second moment are shown in Fig. 1.

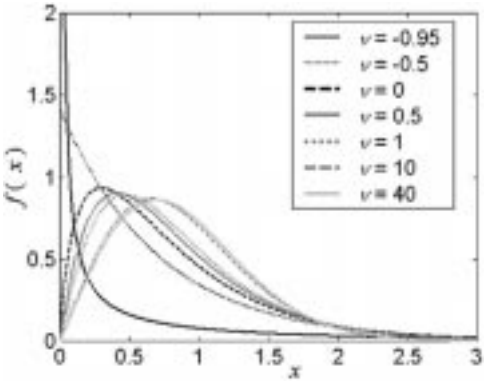

Fig. 1. PDF of the K distribution for various ν.

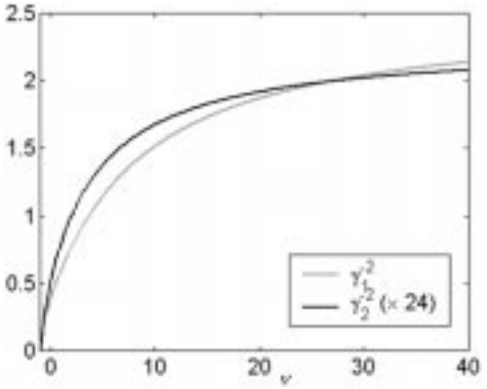

Fig. 2. γ_1^{-2} and γ_2^{-2}.

In the limit, this model approximates Rayleigh statistics as scatterer density becomes large [3]. ν is monotonically related to the number of scatterers, and $\nu + 1$ can be interpreted as the effective number of scatterers in the volume of the medium from which the echo is received [4], [5], [10].

III. Methods

Multilayer perceptrons trained with the backpropagation (BP) learning algorithm were implemented for estimating ν. BP was selected for its fast output generation, in contrast to kernel-based networks (e.g., radial basis function networks).

A. Features

Many current techniques to estimate ν use statistical moments computed from data, as ν can be expressed as a function of moments [4], [5], [9], [11]. The third and fourth standardized central moments, skewness (γ_1) and kurtosis (γ_2), respectively, may be used to characterize

Manuscript received April 3, 2001; revised January 21, 2002. This work was supported in part by the University of Louisville under IRIG Grant 277840. The work of J. M. Zurada was supported in part by the Systems Research Institute of the Polish Academy of Sciences, Warsaw, Poland. *Asterisk indicates corresponding author.*

*M. P. Wachowiak is with the Computer Science and Engineering Program, J.B. Speed Building, Room 123, University of Louisville, Louisville, KY 40292 USA (e-mail: mpwach01@athena.louisville.edu).

R. Smolíková is with the Computer Science and Engineering Program, University of Louisville, Louisville, KY 40292 USA.

J. M. Zurada is with the Department of Electrical and Computer Engineering, University of Louisville, Louisville, KY 40292 USA.

A. S. Elmaghraby is with the Department of Computer Engineering and Computer Science, University of Louisville, Louisville, KY 40292 USA.

Publisher Item Identifier S 0018-9294(02)04852-8.

0018-9294/02$17.00 © 2002 IEEE

TABLE I
E_{RMS} FOR THE TEST DATA, $-1 < \nu \leq 40$ AND $-1 < \nu \leq 10$

Sample size		$N = 100$		$N = 2500$		$N = 10000$	
Method	Parameter	$-1 < \nu \leq 40$	$-1 < \nu \leq 10$	$-1 < \nu \leq 40$	$-1 < \nu \leq 10$	$-1 < \nu \leq 40$	$-1 < \nu \leq 10$
ANN		15.27	9.23	9.46	6.90	20.88	2.91
ML/MOM	$k = 0.5$	> 1000	> 1000	> 1000	635.53	> 1000	2.11
	$k = 1$	> 1000	> 1000	> 1000	65.47	168.54	1.58
	$k = 1.5$	> 1000	> 1000	> 1000	34.78	139.94	1.32
	$k = 2$	> 1000	> 1000	851.70	16.27	104.31	1.16
	$k = 5$	> 1000	> 1000	158.23	2.42	24.31	0.96
LF	$p = 0.25$	> 1000	> 1000	145.56	2.52	22.20	0.96
	$p = 0.5$	> 1000	> 1000	> 1000	23.77	120.54	1.29
	$p = 2$	> 1000	> 1000	> 1000	162.90	515.24	1.44
HF	$p = 0.5$	67.86	49.89	77.45	2.35	36.78	0.90
	$p = 1$	102.24	73.49	106.14	2.27	37.22	0.90
	$p = 1.5$	139.63	114.57	142.15	2.39	49.17	0.94
	$p = 2$	173.68	128.54	165.26	2.62	58.83	1.01
SNR	$p = 0.25$	18.65	9.55	15.80	5.73	13.57	1.56
	$p = 0.33$	18.71	9.52	15.40	5.39	13.22	1.37
	$p = 0.5$	> 1000	> 1000	14.98	3.98	12.42	1.14

TABLE II
σ VALUES FOR (a) $\nu = -0.86$, (b) $\nu = 20.93$, AND (c) $\nu = 39.45$

Sample size		$N = 100$			$N = 2500$			$N = 10000$	
Method	Parameter	A	B	C	A	B	C	A	B	C
ANN		4.09	10.52	9.94	0.17	8.90	6.93	0.06	20.36	27.41
ML/MOM	$k = 0.5$	0.02	> 1000	> 1000	0.00	> 1000	> 1000	0.00	252.25	> 1000
	$k = 1$	0.02	> 1000	> 1000	0.00	617.79	> 1000	0.00	51.52	242.40
	$k = 1.5$	0.02	> 1000	> 1000	0.00	404.11	> 1000	0.00	22.56	206.86
	$k = 2$	0.02	> 1000	> 1000	0.00	228.10	753.46	0.00	12.01	158.71
	$k = 5$	0.02	> 1000	> 1000	0.00	28.24	138.74	0.00	6.97	52.59
LF	$p = 0.25$	0.03	> 1000	> 1000	0.01	46.37	508.85	0.00	24.51	50.26
	$p = 0.5$	0.02	> 1000	> 1000	0.00	612.27	> 1000	0.00	88.87	337.90
	$p = 2$	0.02	> 1000	> 1000	0.00	> 1000	> 1000	0.00	260.68	> 1000
HF	$p = 0.5$	0.04	30.17	70.43	0.01	64.79	146.85	0.00	9.77	122.16
	$p = 1$	0.05	94.29	106.89	0.01	57.79	160.82	0.01	9.54	125.40
	$p = 1.5$	0.08	78.20	114.86	0.02	47.27	343.23	0.01	10.04	104.33
	$p = 2$	0.10	69.22	63.41	0.03	55.08	204.91	0.02	11.62	240.49
SNR	$p = 0.25$	0.01	14.80	12.29	0.00	17.89	17.93	0.00	14.53	16.44
	$p = 0.33$	0.02	17.27	13.89	0.00	17.67	23.93	0.00	14.98	17.77
	$p = 0.5$	> 1000	> 1000	> 1000	0.00	17.25	21.86	0.00	11.12	16.42

the shape of a distribution. As functions of ν, the transformations ${\gamma_1}^{-2}$ and ${\gamma_2}^{-2}$ were found to have a high dynamic range, and were used as input to the ANN. These features are shown in Fig. 2 for $-1 < \nu \leq 40$, where ${\gamma_2}^{-2}$ was scaled for display. The parameter estimation problem is then formulated as: $\hat{\nu} = g({\gamma_1}^{-2}, {\gamma_2}^{-2})$, and the goal of the ANN is to learn the mapping $g(\cdot, \cdot)$.

B. Experiments

1) K Distributed Data: For the specific data and problem under consideration, it was found that an ANN with two hidden layers having ten and five neurons (sigmoidal activation function) was the simplest network with good training and testing results. To reduce the variance in estimates from small sample sizes, separate ANNs were trained for sizes of $N = 100$, 2500, and 10 000.

For training, two K distribution random variates for the three N were generated for each of 200 evenly spaced values of $\nu \in [-0.9, 40]$. K random variates are generated by: $K = 2a\sqrt{G(1, 1)G(\nu + 1, 1)}$, where $G(\alpha, \beta)$ denotes a gamma-distributed random variable with shape parameter α and scale parameter β [11]. a was set to $1/(2\sqrt{\nu + 1})$ so that the second moment was unity (this has no affect on ν). All networks were trained for 200 epochs.

For testing, K variates were generated from 200 random ν values in $[-0.9, 40]$. Estimates were compared to those obtained by the low/fractional order method (LF) [4], the high/fractional order method (HF) [11], the SNR estimator [5], and the maximum-likelihood (ML)/method of moments (MOM) (ML/MOM) approach [9]. These techniques were used with a variety of parameters (denoted as k for ML/MOM, p for other methods), as suggested in the literature. The ML/MOM, LF, and SNR equations were solved numerically with the Newton–Gauss method with line search and with hybrid quadratic

interpolation methods. Matlab (The Mathworks, Inc., Natick, MA) was used for all experiments. Error metrics were root mean squared error (E_{RMS}) and bias.

2) Simulated Envelopes: To test the ability of the estimators to discern scatterer density (ρ), envelope data generated with an ultrasound simulator [12] was utilized. Estimates were computed with the HF, SNR, and ANN estimators. Fifty trials of 60 scatterer densities, with $0.05 \leq \rho \leq 12$ were performed on data of sizes 300, 625, and 1000. Performance was based on the monotonicity (ν increases with scatterer density) and standard deviation of the estimates.

IV. Results

The total E_{RMS} for $-1 < \nu \leq 40$ and for the smaller range $-1 < \nu \leq 10$ (the K scattering model is most appropriate for small densities) is displayed for all N in Table I. Standard deviations for $\nu = -0.86$, 20.93, and 39.45 (three of the randomly generated ν values representing low, midrange, and high parameter values) are shown in Table II. The E_{RMS}, bias, and standard deviation (as a consistency metric) for each ν estimated from data with $N = 2500$ are shown in Fig. 3.

All estimators, including the ANN, are accurate [Fig. 3(a), Table I] and consistent [Fig. 3(c), Table II] for $-0.9 \leq \nu \leq 5$, although the non-ANN estimates were more accurate in this range for $N = 2500$ and $N = 10\,000$. The ANN estimates had the highest standard deviation for $\nu < 1$. For $N = 100$, the ANN and SNR estimators were the most accurate, followed by HF. With increasing ν, the LF and ML/MOM biases increased very rapidly for $\nu > 10$. The ANN, HF, and SNR biases were negative in this range, but decreased slowly. The ANN bias was slightly positive for $5 < \nu < 12$. The ANN estimates had the smallest E_{RMS}, and were the most consistent, for high values of ν and for smaller sample sizes. Although the SNR method generally had very good estimates for all ranges and sample sizes, ν values could not be estimated for some trials due to numerical inaccuracies and the low dynamic range of the SNR functions for large ν. For $N = 100$, 26% of the ν values could not be estimated. For $N = 2500$, the percentage was 17.33%, and for $N = 10\,000$, ν could not be computed for 7.67% of the trials. For $-1 < \nu < 10$, ν was estimated for over 95% of the trials. Numerical problems also contributed to the high errors in the LF and ML/MOM methods.

For the simulated envelopes, mean estimated ν values and their standard deviations for the ANN, SNR, and HF methods are shown in Fig. 4. The estimates from these methods were almost identical for $\rho \leq 1$. For $\rho > 2$, the ANN estimates exhibited greater monotonicity and dynamic range than the SNR and HF methods. For large N, the most accurate and consistent values resulted from $p = 0.5$ for the SNR method, and $p = 0.5$ for the HF technique. Although the SNR estimates were also very good, the numerical solution algorithm did not always converge, as was the case with the K-distributed data. Thus, some of the error in the nonneural methods can be attributed to numerical inaccuracies.

V. Discussion

The ANN and SNR estimates were most accurate and consistent overall. Fig. 4(a) and (c) suggests that the ANN technique may be useful in estimating scatterer density. However, although ANN performance is generally robust in the presence of noise, incorrect generalization may result when features are obtained from data with many outliers. Another consideration is that RF data are not available on many ultrasound systems and, thus, clinical applicability is limited at present. However, as RF data prove increasingly useful, use of imaging systems

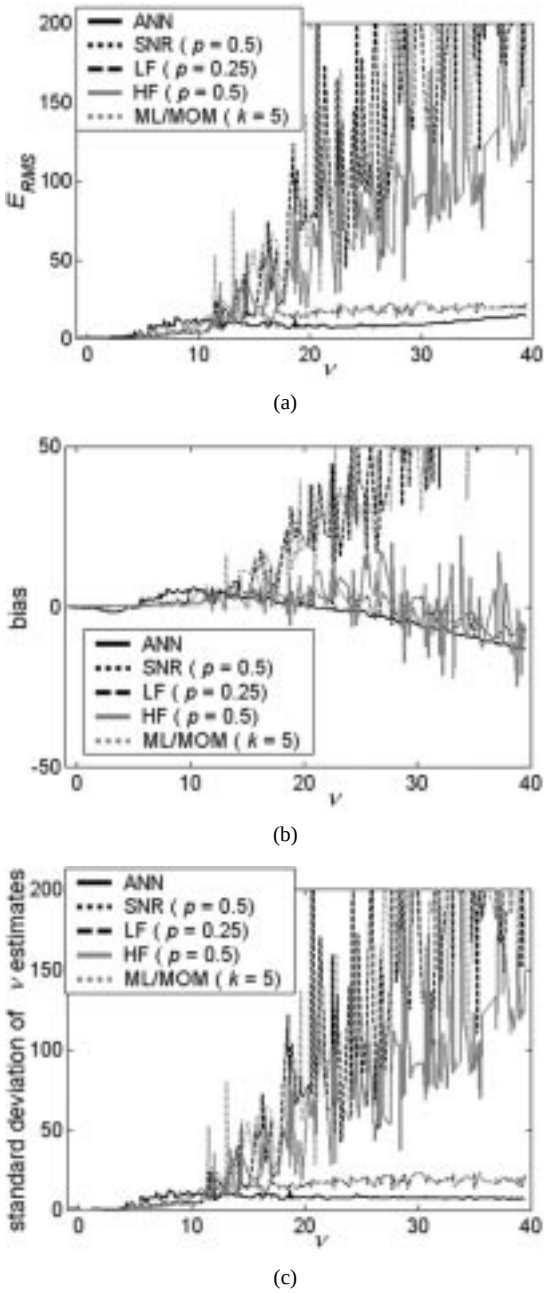

Fig. 3. E_{RMS}, bias and standard deviation of $\hat{\nu}$, $N = 2500$. (a) E_{RMS}, (b) bias, and (c) standard deviation.

providing this data may correspondingly increase. Additionally, information from the echo envelope may be combined with B-scan analysis for more accurate interpretation.

The greatest benefit of the neural approach is in estimating parameters for large ν (high scatterer density, which is possible in ultrasonography) and for small sample sizes. For large N and small ν, the nonneural techniques perform well. The good performance of the ANNs suggest that neural approaches may also be used to estimate parameters from more complex distributions, such as the generalized K distribution, which encompasses post-Rayleigh (SNR > 1.91) as well as pre-Rayleigh and Rayleigh conditions [10]. Although the neural network approach must be validated on clinical ultrasound data, preliminary results strongly suggest that neural estimation can be a complimentary technique in modeling ultrasound backscatter, and may contribute to improving ultrasound analysis and tissue characterization.

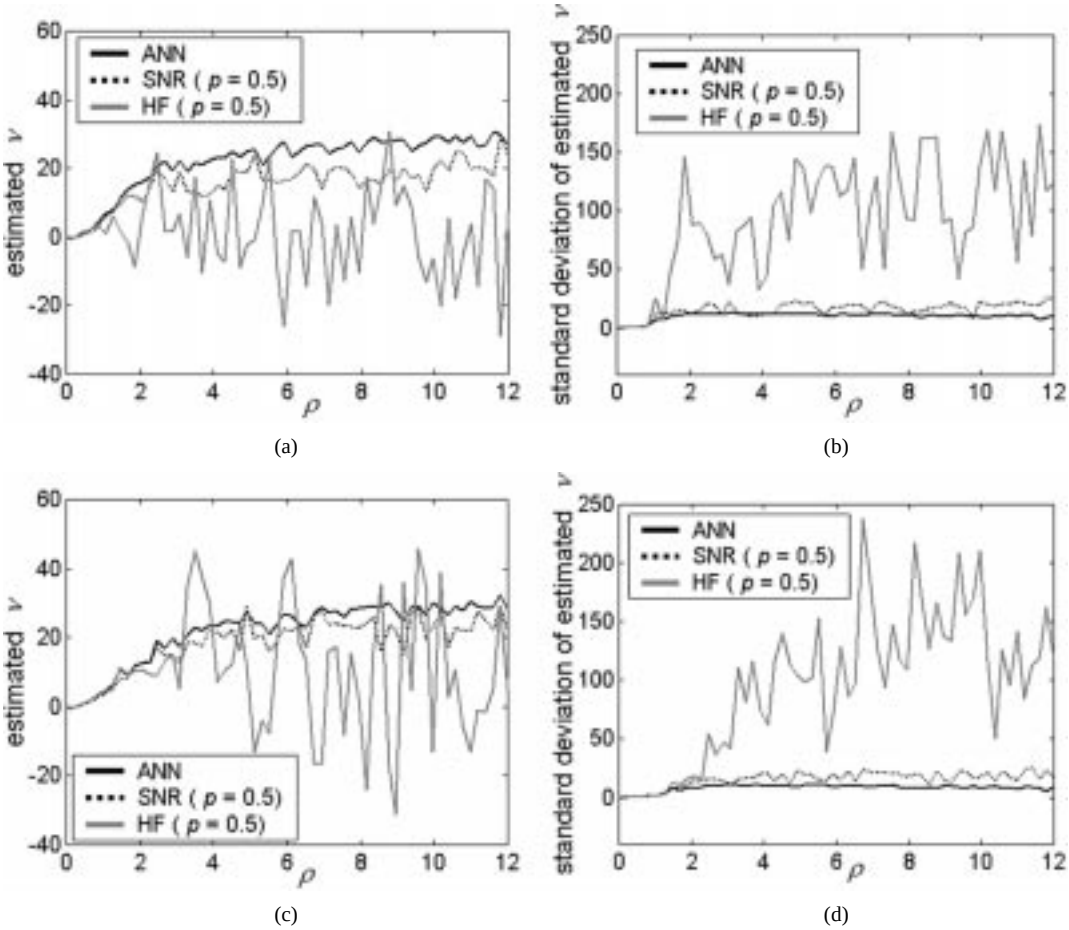

Fig. 4. Mean and standard deviation of $\hat{\nu}$ for simulated echo envelopes. (a) Mean, $N = 300$. (b) Standard deviation, $N = 300$. (c) Mean, $N = 625$. (d) Standard deviation, $N = 625$.

ACKNOWLEDGMENT

The authors would like to thank the reviewers for many helpful comments and suggestions.

REFERENCES

[1] P. M. Shankar, V. A. Dumane, J. M. Reid, V. Genis, F. Forsberg, C. W. Piccoli, and B. B. Goldberg, "Use of the K-distribution for classification of breast masses," *Ultrasound Med. Biol.*, vol. 26, no. 9, pp. 1503–1510, 2000.

[2] L. Clifford, P. Fitzgerald, and D. James, "Non-Rayleigh first-order statistics of ultrasonic backscatter from normal myocardium," *Ultrasound Med. Biol.*, vol. 19, no. 6, pp. 487–495, 1993.

[3] R. C. Molthen, P. M. Shankar, J. M. Reid, F. Forsberg, E. J. Halpern, C. W. Piccoli, and B. B. Goldberg, "Comparisons of the Rayleigh and K-distribution models using *in vivo* breast and liver tissue," *Ultrasound Med. Biol.*, vol. 24, no. 1, pp. 93–100, 1998.

[4] F. Ossant, F. Patat, M. Lebertre, M.-L. Teriierooiterai, and L. Pourcelot, "Effective density estimators based on the K-distribution: Interest of low and fractional order moments," *Ultrason. Imag.*, vol. 20, pp. 243–259, 1998.

[5] V. Dutt and J. F. Greenleaf, "Speckle analysis using signal to noise ratios based on fractional order moments," *Ultrason. Imag.*, vol. 17, pp. 251–268, 1995.

[6] V. Dutt and J. F. Greenleaf, "Ultrasound echo envelope analysis using a homodyned K-distribution signal model," *Ultrason. Imag.*, vol. 16, pp. 265–287, 1994.

[7] I. A. Basheer and M. Hajmeer, "Artificial neural networks: Fundamentals, computing, design, and application," *J. Microbiological Meth.*, vol. 43, no. 1, pp. 3–31, 2000.

[8] R. Rojas, *Neural Networks. A Systematic Introduction.* Berlin, Germany: Springer-Verlag, 1996.

[9] D. R. Iskander, A. M. Zoubir, and B. Boashash, "A method for estimating the parameters of the K-distribution," *IEEE Trans. Signal Processing*, vol. 47, pp. 1147–1151, Apr. 1999.

[10] P. M. Shankar, "A model for ultrasonic scattering from tissues based on the K-distribution," *Phys. Med. Biol.*, vol. 40, no. 10, pp. 1633–1649, 1995.

[11] D. R. Iskander and A. M. Zoubir, "Estimation of the parameters of the K-distribution using higher order and fractional moments," *IEEE Trans. Aerosp. Electron. Syst.*, vol. 35, pp. 1453–1457, Apr. 1999.

[12] H. J. Huisman and J. M. Thijssen, "Adaptive texture feature extraction with application to ultrasonic image analysis," *Ultrason. Imag.*, vol. 20, pp. 132–148, 1998.

A Novel Ferromagnetic Thermo-Stent for Plaque Stabilization That Self-Regulates the Temperature

Takemi Matsui*, Kouji Matsumura, Kousuke Hagisawa, Masayuki Ishihara, Toshiaki Ishizuka, Minoru Suzuki, Akira Kurita, and Makoto Kikuchi

***Abstract*—The purpose of this study is to investigate the vascular wall with a thermally self-regulating, cylindrical stent made of a low Curie temperature ferromagnetic alloy. Physiologic saline was circulated in the silicone model vessel implanted with the stent. The stent-temperature remained nearly constant for variable saline flows, saline temperatures, and magnetic flux densities. Stent implants of this type in human blood vessels could potentially enable thermotherapy and temperature determination without catheterization.**

***Index Terms*—Ferromagnetic, stent, thermo-therapy, vascular.**

I. Introduction

Various types of thermotherapy induced by magnetic fields have been reported in the literature. Ferromagnetic implants with low Curie temperature have been applied to a variety of clinical settings such as tumor therapy [1]–[6]. However, there are no studies, to date, to our knowledge where ferromagnetic stents have been used to heat vascular walls. We developed a novel thermally self-regulating ferromagnetic stent with low Curie temperature (thermo-stent) that can be applied to vascular lumina. The eventual goal of our study is to induce macrophage apoptosis to stabilize atherosclerotic plaques by developing a clinically applicable intravascular ferromagnetic stent [7], [8].

II. Materials and Method

A cylindrical stent was designed for the model experiment. The composition ratio of the palladium and nickel ferromagnetic alloy is 76 : 24 [1]. The outer diameter of the stent is 4 mm, the inner diameter is 3 mm, and the length is 20 mm. The inner surface of the stent is coated with a 0.3-mm-thick plastic film to prevent excessive cooling of the stent by the circulating flow. The stent is 20 mm long. The ferromagnetic alloy has negligible thermal production above the Curie temperature. The stent was implanted into a silicone tube with an inner diameter of 4 mm modeling the blood vessel (Fig. 1). Physiologic saline, warmed to 36 °C in a water bath, was circulated using a tube-pump (Masterflex Co. L/S). The saline temperature was tested for 34 °C to 38 °C simulating the body temperature change. The stent temperature was tested for the saline flow from 17 to 145 ml/min. A magnetic field was generated using an oscillator (Hewlett Packard Co. 33 120A), a radio-frequency (RF) amplifier (ENI Co. 1040), and a coil. Free space was provided between the agar layer and the coil. The 25-KHz alternating current generated by the oscillator was amplified using the RF amplifier. The silicone tube was wrapped with a cylindrical 5-wt% agar (with 0.9-wt% NaCl) layer. The outer diameter of the agar was 20 mm. The agar layer simulates the perivascular tissue around the vessel. The temperature of the ferromagnetic thermo-stent was measured using a thermocouple. The magnetic flux density in the center of the magnet was measured using a solenoid-magnetic sensor. The magnetic flux density was tested from 0 to 12 mT.

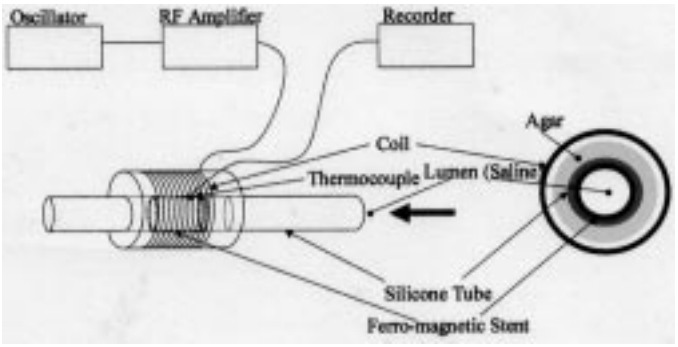

Fig. 1. Schematic diagram of the stent model. The stent was implanted into a silicone tube which simulates a vessel with an inner diameter of 4 mm. The saline was warmed to body temperature in a water bath and circulated using a tube-pump. The 25-KHz alternating magnetic field was irradiated using a coil. The silicone tube was wrapped with a cylindrical 5-wt% agar layer to simulate the perivascular tissue. The magnetic flux density was altered from 0 to 12 mT. The temperature of the ferromagnetic thermo-stent was measured using a thermocouple.

In order to assess the temperature rise of the ferromagnetic thermo-stent under an alternating magnetic field, the thermo-stent was implanted under the livers of five black mice under general anesthesia. The abdomen of each mouse was wrapped with the coil. The alternating magnetic field (25 KHz) was applied for 25 min with a magnetic flux density of 10 mT. The temperature of the implanted thermo-stent was monitored during heating using a thermocouple. The mice were sacrificed and their livers were examined histopathologically.

III. Results

The temperature of the stent gradually reached thermal equilibrium after 500 s by alternating the magnetic field with a flux density of 10 mT (Fig. 2). The temperature of the circulating saline was 36 °C. The flow was 58 ml/min. The temperature of the stent was maintained at 42 °C to 43 °C after 500 s.

After 500 s of alternating magnetic field heating, the temperature of the stent where the temperature of the circulating saline was 36 °C reached thermal equilibrium when the magnetic flux density was above 6 mT (Fig. 3).

The temperature of the stent remained at 42.6 °C at thermal equilibrium with a magnetic flux density of 10 mT when the flow of the saline was altered from 17 to 145 ml/min. The temperature of the circulating saline was 36 °C (Fig. 4).

When the circulating saline temperatures were altered from 34 °C to 38 °C, the temperature of the ferromagnetic thermo-stent increased gradually with rising saline temperature (Fig. 5). The temperature coefficient ($\Delta T_{\rm st}/\Delta T_{\rm sa}$) was 0.05, where $\Delta T_{\rm st}$ was the stent temperature change and $\Delta T_{\rm sa}$ the saline temperature change. The saline flow was 58 ml/min.

The ferromagnetic thermo-stents implanted beneath the livers of the mice had an approximately uniform temperature of 43 °C at thermal equilibrium during alternating magnetic heating. A histologic study on hematoxylin–eosin stained sections revealed that there was no evidence of thermal injuries of the liver resulting from the implanted ferromagnetic thermo-stent.

Manuscript received March 15, 2001; revised January 13, 2002. *Asterisk indicates corresponding author.*

*T. Matsui is with the Division of Biomedical Engineering, Research Institute, National Defense Medical College, 3-2 Namiki, Tokorozawa, Japan (e-mail: matsuit@res.ndmc.ac.jp).

K. Matsumura, K. Hagisawa, M. Ishihara, T. Ishizuka, and A. Kurita are with the Division of Biomedical Engineering, Research Institute, National Defense Medical College, 3-2 Namiki, Tokorozawa, Japan.

M. Suzuki is with the School of Nursing, Kiryu Junior College, Kasakake, azami 606-7, Kiryu, Japan.

M. Kikuchi is with the Department of Medical Engineering, National Defense Medical College, 3-2 Namiki, Tokorozawa, Japan.

Publisher Item Identifier S 0018-9294(02)04853-X.

0018-9294/02$17.00 © 2002 IEEE

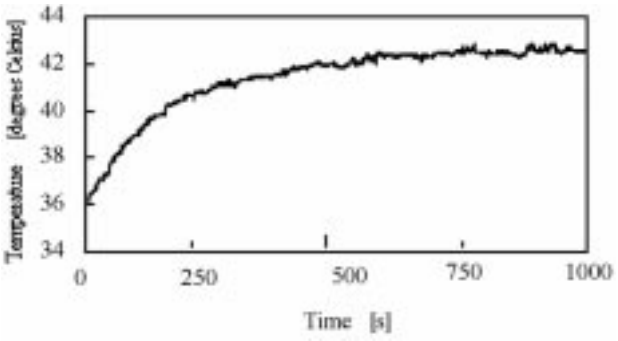

Fig. 2. The time required for temperature stabilization of the stent under 25-KHz magnetic field irradiation. The magnetic flux density was 10 mT, the circulating saline temperature was 36 °C when the flow was 58 ml/min, and the stent temperature was maintained at 42.6 °C thermal equilibrium.

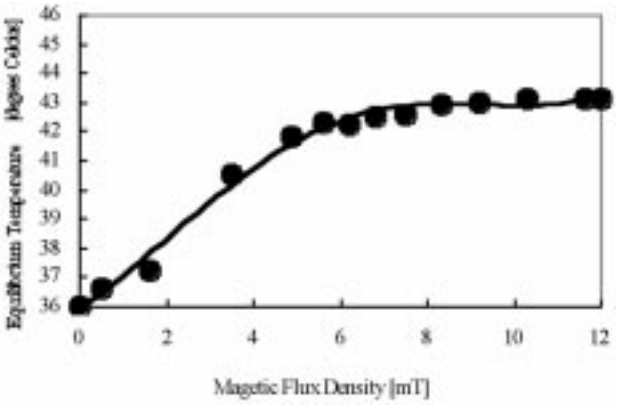

Fig. 3. Effects of the magnetic flux density on thermal equilibrium. The equilibrium temperature of the stent was nearly constant above 6 [mT].

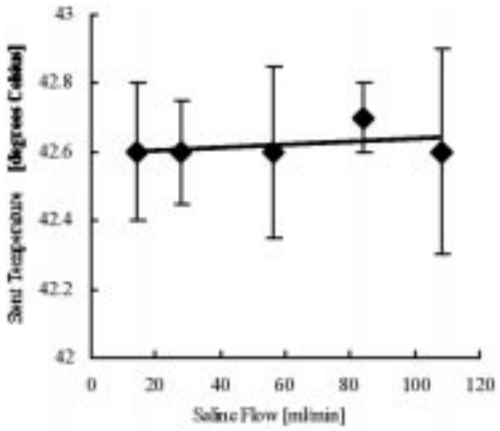

Fig. 4. Effects of the saline flow on the stent temperature. The saline flow was altered from 17 ml/min to 145 ml/min. The temperature remained nearly constant.

IV. Discussion

The temperature of the ferromagnetic thermo-stent was maintained relatively constant under alternating magnetic field heating for various conditions such as the circulating saline flow, the saline temperature, and the magnetic flux density. There was no temperature change of the ferromagnetic stent when the saline flow was altered from 17 ml/min to 145 ml/min. The average human coronary blood flow of 38 ml/min falls within this range [9]. The temperature of the ferromagnetic thermo-stent was nearly constant above 6 mT. The magnetic flux density may change with patient body movement or the location of the magnetic applicator in clinical settings. Our study suggests that the body movement of patients should not affect the temperature of the ferromagnetic thermo-stent during heating. The temperature coefficient ($\Delta T_{\rm st}/\Delta T_{\rm sa}$) was 0.05, where $\Delta T_{\rm st}$ is the stent temperature change and $\Delta T_{\rm sa}$ is the saline temperature change. The temperature change of the ferromagnetic stent resulting from body temperature variation is expected to be smaller than 0.2 °C while the body temperature variation of patients does not exceed 4 °C.

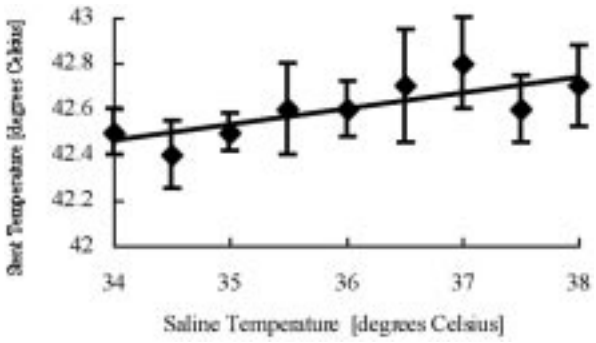

Fig. 5. Effects of the circulating saline temperature on the stent temperature. The temperature of stent rose gradually when the temperature of saline was increased from 34 °C to 38 °C. The temperature coefficient, $\Delta T_{\rm st}/\Delta T_{\rm sa}$ was 0.05, where $\Delta T_{\rm st}$ was the stent temperature change, and $\Delta T_{\rm sa}$ the saline temperature change. The saline flow was 58 ml/min.

After 500 s of the magnetic field heating in this study, the temperature of the stent became stabilized at 42 °C to 43 °C. This high-temperature level above 42 °C should give alleviating effects on atherosclerotic blood vessels because of accelerating macrophage apoptosis [7], whereas in the physiologic temperature range below 40 °C an increase of the local temperature in unstable atherosclerotic plaques was observed [10].

The thermal conductivity of silicone used in this study was approximately 0.73 W $m^{-1}K^{-1}$ compared with 0.50–0.75 W $m^{-1}K^{-1}$ for swine cardiac tissues [11]. The specific heat of blood is approximately 4000 J $kg^{-1}K^{-1}$ which is close to that of water [12].

Ferromagnetic thermo-stents implanted into the blood vessels should enable the future thermo-therapy of patients without catheterization to obtain the temperature measurement.

References

[1] B. Charles, H. Maynard, and A. E. Walker, "The RF thermoseed—A thermally self-regulating implant for the production of brain lesions," *IEEE Trans. Biomed. Eng.*, vol. BME-18, pp. 104–109, 1971.

[2] T. Kobayashi, Y. Kida, N. Kagayama, H. Kobayashi, and Y. Amemiya, "Magnetic induction hyperthermia for brain tumor using ferromagnetic implant with low Curie temperature," *J. Neuro-Oncol.*, vol. 4, pp. 175–181, 1986.

[3] H. Matsuki, K. Murakami, and H. Niizuma, "Soft heating—A new method of heating temperature-sensitive magnetic materials," *IEEE Trans. Magn.*, vol. MAG-18, pp. 1788–1790, 1982.

[4] M. Matsumoto, N. Yoshimura, Y. Honda, M. Hiraoka, and K. Ohura, "Ferromagnetic hyperthermia in rabbit eyes using a new glass–ceramic thermoseed," *Graef. Arch. Clin. Exp.*, vol. 232, pp. 176–181, 1994.

[5] K. Takegami, T. Sano, H. Wakabayashi, J. Sonoda, T. Yamazaki, S. Morita, T. Shibuya, and A. Uchida, "New ferromagnetic bone cement for local hyperthermia," *J. Biomed. Mater. Res.*, vol. 43, pp. 210–214, 1998.

[6] J. G. Meijer, N. van Wieringen, C. Koedooder, G. J. Nieuwenhuys, and J. D. van Dijk, "The development of Pd/Ni thermoseeds for interstitial hyperthermia," *Med. Phys.*, vol. 22, pp. 101–104, 1995.

[7] K. Gul, M. S. Naghavi, W. Saidaty, W. Casscells, A. Chen, and J. T. Willerson, "*In vivo* physiologic heating of rabbit atherosclerotic plaques," *J. Amer. Coll Cardiol.*, vol. 35, 244A, 2000.

[8] J. P. Strong, "Atherosclerotic lesions. Natural history, risk factors, and topography," *Arch. Pathol. Lab. Med.*, vol. 116, pp. 1268–1275, 1992.

[9] C. P. Davis, P. F. Liu, M. Hauser, S. C. Gohde, G. K. Schulthess, and J. F. Debatin, "Coronary flow reserve measurements in humans with breath-held magnetic resonance phase contrast velocity mapping," *Magn. Reson. Med.*, vol. 37, pp. 537–544, 1997.

[10] C. Stefanadis, L. Diamantopoulos, C. Lachopoulos, E. Tsiamis, J. Dernellis, and P. Toutouzas, "Thermal heterogeneity within human atherosclerotic coronary arteries detected *in vivo*: A new method of detection by application of a special thermography catheter," *Circulation*, vol. 99, pp. 1965–1971, 1999.

[11] N. C. Bhavaraju, H. Cao, D. Y. Yuan, J. W. Valvano, and J. G. Webster, "Measurement of directional thermal properties of biomaterials," *IEEE Trans. Biomed. Eng.*, vol. 48, pp. 261–267, Feb. 2001.

[12] J. Liu and L. X. Xu, "Boundary information based diagnostics on the thermal states of biological bodies," *Int. J. Heat Mass Tran.*, vol. 43, pp. 2827–2829, 2000.